濟州大學校 尖端技術硏究所 論文集, 第12卷, 2號, pp.174-180, 2001. 12
Cheju Nat'l Univ. Res. Inst. Adv. Tech. Jour., Vol.12, No.2, pp.174-180, 2001. 12

Electrical Impedance Tomography Reconstruction Algorithm Using Extended Kalman Filter

Ho-Chan Kim*, Kyung-Youn Kim*, Jae-Woo Park**, Heon-Ju Lee**

확장 Kalman 필터에 의한 전기임피던스 영상복원 알고리즘

김 호 찬* · 김 경 연* · 박 재 우** · 이 헌 주**

ABSTRACT

In electrical impedance tomography (EIT), the internal resistivity distribution of the unknown object is estimated using the boundary voltage data induced by different current patterns using various reconstruction algorithms. This paper presents a reconstruction algorithm based modified extended Kalman filter technique that is able to track fast change in the impedance distribution. The computer simulation for the 32 channels synthetic data shows that the reconstruction performance of the proposed scheme is improved compared to that of the conventional Kalman filter algorithm at the expense of slightly increased computational burden.

Key Words : electrical impedance tomography, modified extended Kalman filter

I. INTRODUCTION

Electrical impedance tomography (EIT) plays an important role in monitoring tools for the process engineering such as biomedical, geological and chemical engineering, due to its relatively cheap electronic hardware requirements and non-intrusive measurement properties[1-3]. In EIT different current patterns are injected to the unknown object through electrodes and the corresponding voltages are measured on its boundary surface. The physical relationship between inner resistivity (or conductivity) and boundary surface voltage is governed by the nonlinear Laplace equation with appropriate boundary conditions so that it is impossible to obtain the closed-form solution for the resistivity distribution. Hence, the internal resistivity distribution of the unknown object is estimated using the boundary voltage data based on various reconstruction algorithms.

Yorkey et al.[4] developed a modified

* 제주대학교 전기전자공학부, 첨단기술연구소
Faculty of Electrical & Electronic Engineering, Research Institute of Advanced Technology, Cheju Nat'l Univ.
* 제주대학교 에너지공학과, 첨단기술연구소
Department of Nuclear and Energy Engineering, Research Institute of Advanced Technology, Cheju Nat'l Univ.

Newton- Raphson (mNR) algorithm for a static EIT image reconstruction and compared it with other existing algorithms such as backprojection, perturbation and double constraints methods. They concluded that the mNR reveals relatively good performance in terms of convergence rate and residual error compared to that of the other methods.

However, in real situations, the mNR method is often failed to obtain satisfactory images from physical data due to large modeling error, poor signal to noise ratios (SNRs) and ill-conditioned (ill-posed) characteristics. That is, the ratio between the maximum and minimum eigenvalues of the information matrix (or Hessian matrix) is very large. In particular, the ill-conditioning of the information matrix results in an inaccurate matrix inverse so that the resistivity update process is very sensitive to the modeling and measurement errors.

The dynamical reconstruction algorithm proposed in this paper is based on the state-space representation of the dynamical EIT. The state of the system, i.e., the resistivity distribution, is re-estimated after the voltage measurements corresponding to each current pattern. We can thus obtain reconstructions 31 times faster than with the conventional methods (when 31 current patterns with 32 electrodes are used). The method is based on the formulation of EIT as a state-estimation problem and the recursive estimation of the state with the aid of the Kalman filter[5,6].

In this paper, we develop a modified extended Kalman filter algorithm with a time-varying linearized model to track fast changes of impedance in dynamic EIT. The Kalman filter approach has been used here, since it is capable of producing estimates after the injection of each current pattern. We evaluate the performance of the proposed algorithm by simulations.

II. MATHEMATICAL MODEL OF EIT

2.1. The Forward Problem

When electrical currents $I_l(l=1,\cdots,L)$ is injected into the object $\Omega\in R^2$ through electrodes $e_l(l=1,\cdots,L)$ attached on the boundary $\partial\Omega$ and the resistivity distribution $\rho(x,y)$ is known for the Ω, the corresponding induced electrical potential $u(x,y)$ can be determined uniquely from the nonlinear Laplace equation which can be derived from the Maxwell equation, Ohm's law, and the Neumann type boundary condition. The complete electrode model takes into account both the shunting effect of the electrode and the contact impedances between the electrodes and tissue. The equations of complete electrode model are

$$\nabla\cdot(\rho^{-1}\nabla u)=0 \text{ in } \Omega \tag{1}$$

$$\begin{aligned}&\int_{e_l}\rho^{-1}\frac{\partial u}{\partial n}dS=I_l,\ l=1,\cdots,L\\ &u+z_l\rho^{-1}\frac{\partial u}{\partial n}=U_l \text{ on } e_l,\ l=1,\cdots,L\\ &\rho^{-1}\frac{\partial u}{\partial n}=0 \text{ on } \partial\Omega\setminus\bigcup_{l=1}^{L}e_l\end{aligned} \tag{2}$$

where z_l is effective contact impedance between l th electrode and tissue, U_l are the measured potentials and n is outward unit normal. In addition, we have the following two conditions for the injected currents and measured voltages by taking into account the conservation of electrical charge and appropriate selection of ground electrode, respectively.

$$\sum_{l=1}^{L}I_l=0\cdot \tag{3}$$

$$\sum_{l=1}^{L}U_l=0\cdot \tag{4}$$

The computation of the potential $u(x,y)$ for the given resistivity distribution $\rho(x,y)$ and boundary condition I_l is called the forward problem. The numerical solution for the forward problem can be obtained using

the finite element method (FEM). In the FEM, the object area is discretized into small elements having a node at each corner. It is assumed that the resistivity distribution is constant within an element. The potential at each node is calculated by discretizing (1) into $Yv = c$, where $Y \in R^{N \times N}$ is so-called stiffness matrix and N is the numbers of FEM nodes. Y and c are the functions of the resistivity distribution and the injected current patterns, respectively.

2.2. The Inverse Problem

The inverse problem, also known as the image reconstruction problem, consists in reconstructing the resistivity distribution $\rho(x, y)$ from potential differences measured on the boundary of the object. In the past, several EIT image reconstruction algorithms for the current injection method have been developed by various authors. A review of these methods is given in[7]. To reconstruct the resistivity distribution inside the object, we have to solve the nonlinear ill-posed inverse problem. The regularization techniques are needed to obtain stable solutions due to the ill-posedness.

Generalized Tikhonov regularized version of the EIT inverse problem can be written in the form

$$\Phi(\rho) = \min_{\rho} \{ \| V - U(\rho) \|^2 + \alpha \| R(\rho - \rho^*) \|^2 \}, \quad (5)$$

where $\rho \in R^N$ and ρ^* are the resistivity distribution and *a priori* information of ρ, respectively. $U(\rho) \in R^{LK}$ is the vector of voltages obtained from the model with known ρ. $V \in R^{LK}$ are the measured voltages and R and α are the regularization matrix and the regularization parameter, respectively. L, K, and M are the numbers of electrodes on the surface, injected current patterns, and finite elements in FEM respectively. There are many approaches in the literature[8-11] to determine R and α, but the usual choice is to fix $R = I_N$ and to adjust α empirically.

In the linearized approach, $U(\rho)$ is approximated with the first order Taylor polynomial at ρ_t as

$$U(\rho) = U(\rho_t) + J(\rho_t)(\rho - \rho_t), \quad (6)$$

where ρ_t and $J(\rho_t) \equiv \left. \frac{\partial U(\rho)}{\partial \rho} \right|_{\rho = \rho_t} \in R^{LK \times N}$ are the resistivity distribution at time t and the Jacobian of $U(\rho) \in R^{LK}$ calculated in ρ_t, respectively. We can write (6) in the form

$$U(\rho_t) = \left(U_{1,t}, \cdots, U_{K,t} \right)^T, \quad J(\rho_t) = \left(J_{1,t}, \cdots, J_{K,t} \right)^T \quad (7)$$

where $U_{k,t} \equiv U_k(\rho_t) \in R^L$ and $J_{k,t} \equiv J_k(\rho_t) \in R^{L \times N}$ for all k. In (7), the kth block corresponds to the current pattern I_k. In a dynamical situation, the measurements $U_{1,t}, \cdots, U_{K,t}$ do not correspond to the same impedance distribution since the distribution changes over time during the measurement cycle. We assume, however, that the evolution of the impedance is so slow that the measurements that correspond to a single current pattern can be taken to be approximately from the same distribution. This is a qualitative requirement, in exact terms this would mean that we have an EIT system that is capable of parallel voltage measurements. Let the current pattern at time t be I_t so that it is one of the patterns $I_1, \cdots, I_K$. The corresponding measurement voltages at time t are defined by $V(t) = \left(V_1(t), \cdots, V_K(t) \right)^T$. The observation equation at time t can be written in the form

$$V_k(t) = U_k(\rho_{t_0}) + J_{k,t_0}(\rho_t - \rho_{t_0}) + w_t \quad (8)$$

where ρ_{t_0} is the resistivity distribution at time t_0 and w_t is the measurement noise, whose covariance is denoted by .

If we define a variable y_t as follows,

$$y_t \equiv V_k(t) - U_k(\rho_{t_0}) + J_{k,t_0} \rho_{t_0}$$

then a new observation equation can be written as

$$y_t = J_{k,t_0}\rho_t + w_t \tag{9}$$

Furthermore, a pseudo-measurement vector and matrix are augmented by (10) to consider the regularization term in (5).

$$\overline{y_t} \triangleq \begin{pmatrix} y_t \\ \sqrt{\alpha}R\rho^* \end{pmatrix}, \quad H_t \triangleq \begin{pmatrix} J_{k,t_0} \\ \sqrt{\alpha}R \end{pmatrix} \tag{10}$$

We describe the evolution of ρ_t with the discrete-time model using nonlinear mapping

$$\rho_{t+1} = G(\rho_t) \tag{11}$$

$G(\rho_t)$ also can be approximated with the first order Taylor polynomial at ρ_{t-1} as

$$G(\rho_t) = G(\rho_{t-1}) + G'(\rho_{t-1})(\rho_t - \rho_{t-1}) + O(\|\rho_t - \rho_{t-1}\|^2) \tag{12}$$

If the second order terms are dropped out in (12) and the result of $\rho_t = G(\rho_{t-1})$ is used in (11), we can describe the time-varying linearized model (state equation)

$$\delta\rho_{t+1} = F_t\delta\rho_t + v_t \tag{13}$$

where $\delta\rho_{t+1} = \rho_{t+1} - \rho_t$, $\delta\rho_t = \rho_t - \rho_{t-1}$ and $F_t \triangleq \left.\frac{\partial G(\rho)}{\partial\rho^T}\right|_{\rho=\rho_t} \cong \frac{\delta\rho_t}{\delta\rho_{t-1}} \in R^{N\times N}$ is the state transition matrix at time t. v_t are the state noise process, whose covariance is denoted by $\Gamma_{v,t} = E(v_t v_t^T)$.

III. IMAGE RECONSTRUCTIONS USING EXTENDED KALMAN FILTER METHOD

Equations (8) and (13) construct the so-called state space representation of the linearized EIT system. Denote the estimate of ρ_t that is based on the observations $U(\rho_1),\cdots,U(\rho_k)$ by $\rho_{t|k}$. The most common recursive estimators of the state ρ_t are called the Kalman predictor ($\rho_{t|t-1}$), filter ($\rho_{t|t}$) and smoother ($\rho_{t|T}$). A Kalman filter is formulated when the relationship between measurements and the state variable is expressed by a linear function. When the relationship between measurements and the state variables is expressed by a nonlinear function, an extended Kalman filter (EKF)[12] is used, where the nonlinear function is approximated as linear and the Kalman filter is applied using this function.

In this paper, we use a modified extended Kalman filter (MEKF)[13] in the form, which compensates for the influence of error due to linear approximation.

$$\begin{aligned} \delta\rho_{t+1|t} &= F_{t|t}\delta\rho_{t,t} \\ P_{t+1|t} &= F_{t|t}P_{t|t}F_{t|t}^T \end{aligned} \tag{14}$$

$$\begin{aligned} K_t &= P_{t|t-1}H_{t|t-1}^T\left(H_{t,t-1}P_{t|t-1}H_{t|t-1}^T + \Gamma_{w,t}\right)^{-1} \\ \delta\rho_{t,t} &= \delta\rho_{t|t-1} + \beta K_t(\overline{y_t} - H_{t|t-1}\rho_{t|t-1}) \\ P_{t|t} &= P_{t|t-1} - \gamma^2 K_t H_{t|t-1}P_{t|t-1} \end{aligned} \tag{15}$$

$$\gamma = \begin{cases} \beta; 0 \le \beta \le 1 \\ 2-\beta; 1 \le \beta \le 2 \end{cases} \tag{16}$$

where

$$F_{t,t} = \left.\frac{\partial G(\rho)}{\partial\rho^T}\right|_{\rho=\rho_{tt}},$$

$$H_{t|t-1} = \begin{pmatrix} J_{k,t|t-1} \\ \sqrt{\alpha}R \end{pmatrix},$$

$$J_{k,t|t-1} = \left.\frac{\partial U(\rho)}{\partial\rho^T}\right|_{\rho=\rho_{tt-1}}, \text{ and}$$

$$\overline{y_t} = \begin{pmatrix} V_k(t) - U_k(\rho_{t|t-1}) + J_{k,t|t-1}\rho_{t|t-1} \\ \sqrt{\alpha}R\rho^* \end{pmatrix}.$$

Let us consider the meaning of coefficient β here. When $\beta = 1$, (14) and (15) are the same as EKF. If the cost function of (5) is the minimum when $\beta = 1$, this means that the nonlinearity of the system is small, and that error caused by linear approximation is small. If the position where the cost function (5) becomes the minimum is distance from $\beta = 1$, the error caused by linear approximation is large.

When $\beta = 0$, the state is not updated even if new measurements are input. This means that it is sufficient to search the position

where the cost function becomes the minimum in the range of $0 \le \beta \le 1$, with $\beta = 1$ at the center. The update value of the error covariance matrix of (15) is $\gamma = 1$ when $\beta = 1$, and γ is decreased as β becomes distance from 1.

IV. RESULTS AND DISCUSSION

In order to test the proposed algorithm, the complete electrode model with the finite element method (FEM) was used to calculate the measurements V. For the current injection the trigonometric current patterns were used. For the forward calculations, the domain Ω is the unit disc and the mesh of 3104 triangular elements (M=3104) with 1681 nodes (N=1681) and 32 channels (L=32) was used as shown in Fig. 1(a). The FEM elements are grouped together such that a total of 776 elements (M=776) with 453 nodes (N=453) were obtained for the inverse calculations as shown in Fig. 1(b).

The inverse problem was solved using both the proposed extended Kalman filter (EKF) algorithm with a time-varying linearized model and the conventional linearized Kalman filter (LKF) algorithm with a random-walk model to compare the resistivity reconstruction performance. We injected 31 trigonometric current patterns and assumed that initial resistivity distribution was the same as background resistivity value (that is, *a priori* information ρ^* about the true resistivity distribution is not used). The parameters used in solving the inverse problem are selected as follows; The regularization matrix and parameter for both algorithms are set to the same as $R = I_N$ and $\alpha = 0.5$. The parameters of the Kalman filter that were used in the calculations are equal to $\Gamma_{w,t} = 10 I_N$ for all t, $\Gamma_{v,t} = 10^{-3} I_L$ for all t and $P_{1|0} = I_N$. The scaling factor coefficients in MEKF are $\beta = 0.9$ and $\gamma = 0.9$. In the reconstruction the voltage mapping was linearized at the time average of the resistivity distribution. These values were 300 Ωcm for the background and 600 Ωcm for the target.

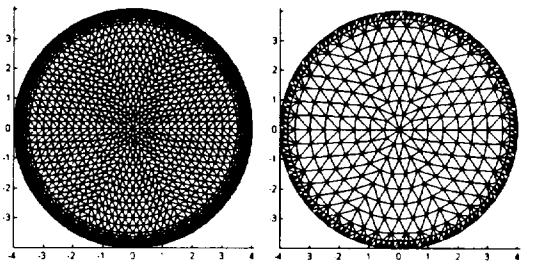

(a) (b)

Fig. 1. The finite element mesh used in the calculations.
(a) mesh for forward solver,
(b) mesh for inverse solver.

Figure 2 show reconstructed dynamic images using the LKF and EKF algorithms. The true targets in both figures consist of one insulator rod as shown in Figs. 2(a). A 45° rotated insulator rod was appeared every 8 current patterns. Figs. 2(b) and Figs. 2(c) were reconstructed by the conventional LKF algorithm with a random-walk model and the proposed EKF algorithm with a time-varying linearized model. The images from the LKF algorithm in Figs. 2(b) showed uniform internal layers and a blurred object than that in Figs. 2(c). In contrast, the images from the EKF algorithm in Figs. 2(c) have an accurately reconstructed the location and size of the insulator rod. This implies that modeling time-varying linearized function accurately helps to improve the performance of reconstruction algorithms.

VI. CONCULSION

In this paper, we developed an extended Kalman filter algorithm to obtain accurate reconstruction images that are capable of

faster tracking of impedance changes. For the evolution of resistivity distribution ρ_t at time t, we use a time-varying linearized model instead of random-walk model. The proposed algorithm has better reconstruction performance than the conventional linearized Kalman filter scheme with a random-walk model at the expense of increased computational burden. Further extensions include a more appropriate state evolution model and adaptive mesh grouping method for accurate image reconstructions.

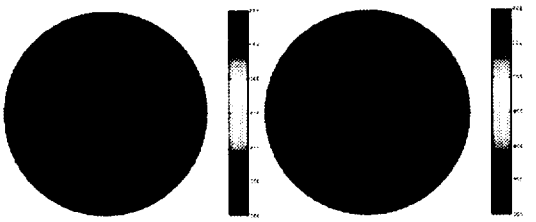

<8 step of 1st frame> <32 step of 1st frame>

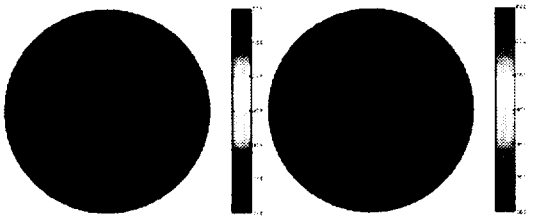

<8 step of 2nd frame> <32 step of 2nd frame>

(a)

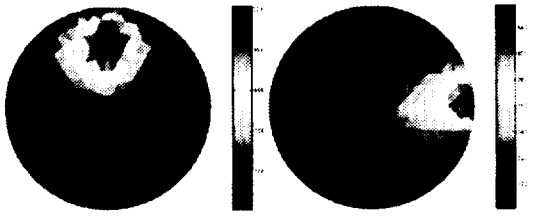

<8 step of 1st frame> <32 step of 1st frame>

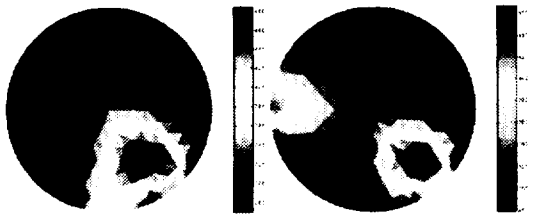

<8 step of 2nd frame> <32 step of 2nd frame>

(b)

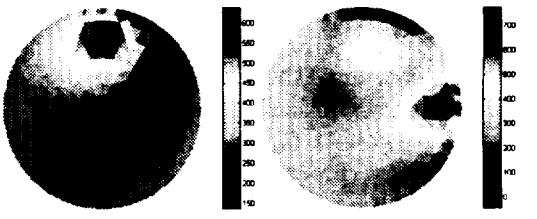

<8 step of 1st frame> <32 step of 1st frame>

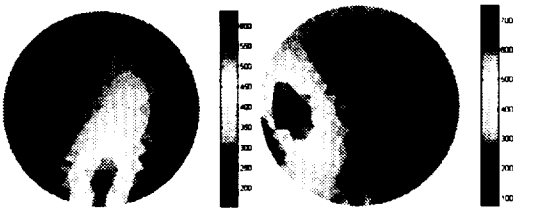

<8 step of 2nd frame> <32 step of 2nd frame>

(c)

Fig. 2. Reconstructed dynamic images using the FEM. model.
(a) The original images.
(b) Reconstructed images by LKF.
(c) Reconstructed images by EKF.

요 약

전기임피던스 단층촬영기법이란 영상복원 알고리즘을 이용하여 다양한 패턴의 주입전류에 의해 여기된 전압을 측정함으로써 미지의 대상체 내부의 저항분포를 추정하는 기법을 말한다. 본 논문에서는 개선된 확장 Kalman filter를 이용한 영상복원 알고리즘을 소개한다. 개선된 확장 Kalman filter은 빠르게 변화하는 임피던스 분포를 추적할 수 있는 장점이 있다. 32채널 EIT 장치에서 전산 실험을 통해 얻은 합성 데이터를 이용하여 본 연구에서 제시한 알고리즘과 기존 Kalman filter를 비교한 결과, 약간의 계산 부하가 추가되었으나 전체적으로 영상복원 능력이 개선되었음을 확인하였다.

ACKNOWLEDGEMENTS

This study was sponsored by Nuclear Academic Research Program by Ministry of Science & Technology (MOST).

REFERENCES

1) J. G. Webster, 1990. Electrical Impedance Tomography, Adam Hilger.
2) J. C. Newell, D. G. Gisser, and D. Isaacson, 1987. An Electric Current Tomograph, IEEE Trans. on Biomedical Engineering, vol. 35, pp. 828-833.
3) M. Cheney, D. Isaacson, and J. C. Newell, 1999. Electrical Impedance Tomography, SIAM Review, vol. 41, pp. 85-101.
4) T. J. Yorkey, J. G. Webster, and W. J. Tompkins, 1987. Comparing Reconstruction Algorithms for Electrical Impedance Tomography, IEEE Trans. on Biomedical Engineering, vol. 34, pp. 843-852.
5) M. Vauhkonen, P. A. Karjalainen, and J. P. Kaipio, 1998. A Kalman Filter Approach to Track Fast Impedance Changes in Electrical Impedance Tomograpy, IEEE Trans. on Biomedical Engineering, vol. 45, pp. 486-493.
6) M. Vauhkonen, P. A. Karjalainen, and J. P. Kaipio, 1998. A Kalman Filter Approach Applied to the Tracking of Fast Movements of organ boundaries, Proc. of 20th Conference of the IEEE Engineering in Medicine and Biology Society, vol. 20, pp. 1048-1051.
7) T. Murai and Y. Kagawa, 1985. Electrical impedance Computed Tomography Based on a Finite Element Model, IEEE Trans. on Biomedical Engineering, vol. 32, pp.177-184.
8) C. Cohen-Bacrie, Y. Goussard, and R. Guardo, 1997. Regularized Reconstruction in Electrical Impedance Tomography Using a Variance Uniformization Constraint, IEEE Trans. on Medical Imaging, vol. 16, pp. 170-179.
9) M. Vauhkonen, D. Vadasz, P. A. Karjalainen, and J. P. Kaipio, 1996. Subspace Regularization Method for Electrical Impedance Tomography, 1st International Conference on Bioelectromagnetism, Tampere, Finland, pp. 9-13.
10) A. Adler and R. Guardo, 1996. Electrical Impedance Tomography: Regularized Imaging and Contrast Detection, IEEE Trans. on Medical Imaging, vol. 15, pp. 170-179.
11) C. J. Grootveld, A. Segal, and B. Scarlett, 1998. Regularized Modified Newton-Raphson Technique Applied to Electrical Impedance Tomography, John Wiley & Sons, International Journal of Imaging System Technology, vol. 9, pp. 60-65.
12) M. S. Grewal and A. P. Andrews, 2001. Kalman Filtering: Theory and Practice using MATLAB, Wiley International.
13) O. Fujimoto, Y. Okita, and S. Ozaki, 1997. Nonlinearity Compensation Extended Kalman Filter and its Application to Target Motion Analysis, Oki Technical Review, vol. 63.